Supporting Information

Fe-N_x sites coupled with Fe_3C on porous carbon from plastic wastes for oxygen reduction reaction

Xiaole Jiang‡ [a], Rui Zhang‡ [a], Qingqing Liao[a], Hanjun Zhang[a], Yaoyue Yang[a], Fan Zhang* [b]

[a] Laboratory of Fundamental Chemistry of the State Ethnic Commission, School of Chemistry and Environment, Southwest Minzu University, Chengdu 610041, China

[b] Key Laboratory of Green Chemistry and Technology, Ministry of Education, National Engineering Laboratory of Eco-Friendly Polymeric Materials (Sichuan), College of Chemistry, Sichuan University, Chengdu 610065, China.

‡ These authors contributed equally to this work.

List of Contents

Materials and methods

1. Materials and chemicals

Polyethylene terephthalate (PET) was purchased from Xing wang Plastic Material Co. Ltd. (China). Cyanoguanidine (DCD, ≥99%) was obtained from Shanghai Titan Scientific Co., Ltd. Magnesium oxide (MgO) nanoparticles, perchloric acid ($HClO_4$, 70~72%) and nitric acid (HNO_3, 65~68%) were purchased from Chengdu Shu Test Biotechnology Co., Ltd. Iron(II) chloride anhydrous ($FeCl_2$, ≥99.5%) was obtained from Shanghai Macklin Biotechnology Co., Ltd. 1,10-phenanthroline monohydrate ($C_{12}H_8N_2 \cdot H_2O$, ≥98%) and potassium hydroxide (KOH, ≥85%) were purchased from Shanghai Aladdin Biochemical Technology Co., Ltd. Commercial Pt/C (40 wt.%) was purchased from Johnson Matthey.

2. Characterizations

The pyrolysis behavior of PET/MgO/DCD mixture was determined on a thermogravimetric analyzer (TGA, HCT-3, HengJiu, China). The X-ray diffraction (XRD) patterns of all the catalysts were obtained using an X-ray diffractometer (Rigaku, Ultima IV) with Cu Kα radiation (λ= 0.15418 nm). The morphology and microstructure of the catalysts were investigated by scanning electron microscopy (SEM, Thermo Scientific Apreo 2S) and transmission electron microscopy (TEM, JEOL-JEM 2100F). Raman spectra of all the catalysts were collected by a Horiba LabRAM HR Evolution Raman spectrometer with a 532 nm laser. The chemical states and surface compositions of the catalysts were analyzed by X-ray photoelectron spectrometer (XPS, ESCALAB 250Xi, Thermo Fisher Scientific). All the binding energies were calibrated by the C 1s peak at 284.8 eV. The N_2 adsorption/desorption isotherms were measured at 77 K with a Quantachrome Autosorb-iQ instrument. The specific surface area and pore size distribution were calculated by the Brunauer-Emmett-Teller (BET) and QSDFT method.

3. Synthesis of catalysts

3.1 Synthesis of N-C from PET

Firstly, PET power was blended with DCD and MgO with a mass ratio of 1:1:9. Then, the mixture was pyrolyzed at 900 °C for 1 h under Ar atmosphere. The resulting product was etched by 0.5 M HNO_3 at room temperature for 16 h, and the final sample named N-C was obtained after washing with deionized water and drying at 80 °C."

3.2 Synthesis of Fe_3C/Fe-N-C and Fe-N-C

Typically, 0.32 mmol $FeCl_2$ and 1 mmol 1,10-phenanthroline monohydrate were dissolved in 5 mL of deionized water. The solution quickly became a blood-red color, confirming the formation of the Fe-Phen complex. Then 0.2 g of N-C was dispersed in 35 mL of deionized water, and added into the Fe-Phen complex solution, followed by sonication for 2 h. After stirring for 24 h at room temperature, the Fe-Phen/N-C composites were obtained via freeze drying. Subsequently, the obtained Fe-Phen/N-C composites were pyrolyzed at 1000 ℃ for 1 h under an Ar atmosphere. Finally, the products were acid-leached by 0.5 M $HClO_4$ at 80 ℃ for 16 h, and the Fe_3C/Fe-N-C catalyst was obtained after the washing and drying process. For comparison, the Fe-N-C catalyst was synthesized with a similar procedure, except that the pyrolyzed temperature was 700 ℃.

4. Electrochemical measurement

The electrochemical measurements were carried out with rotating ring-disk electrode (DC-DSR ROTATOR， PHYCHEMI). Glassy carbon (GC) electrodes coated with the catalysts served as the working electrode. 5 mg of electrocatalyst was dispersed in a mixture of 2 ml of ethanol and 50 ul of Nafion solution (5 wt.%). Then, 25 ul of electrocatalyst ink was deposited onto the polished GC with a catalyst loading of 0.3 mg cm^{-2}. A Hg/HgO and graphene rod acted as reference electrode and counter electrode, respectively.

The ORR performance of all the catalysts was evaluated in an O_2-saturated 0.1 M KOH solution. Linear sweep voltammetry (LSV) measurements were carried out by using rotating disk electrode (RDE) with different rotation speeds (400, 600, 900, 1200

and 1600 rpm) at a scan rate of 10 mV s^{-1}. All the potentials in this work refer to reversible hydrogen electrode (RHE) by using the equation E(RHE)=E(Hg/HgO) +0.98+0.059×pH. The kinetic current density (J_K) and electron transfer number (n) were calculated according to the Koutecky-Levich (K-L) equation:

$$\frac{1}{J}=\frac{1}{J_L}+\frac{1}{J_K}=\frac{1}{\mathrm{B}\omega^{\frac{1}{2}}}+\frac{1}{J_K} \quad (1)$$

$$\mathrm{B}=0.62nFC_0D_0^{\frac{2}{3}}v^{-\frac{1}{6}} \quad (2)$$

where J is the experimentally measured current density, J_k and J_L are the kinetic current density and diffusion-limited current density, ω is the angular velocity (ω=2πN, N is the rotation rate), F is Faraday constant (96485 C·mol^{-1}), n is the electron transferred number, C_0 is the concentration of O_2 in the electrolyte (1.2 × 10^{-6} mol·cm^{-3}), D_0 is the diffusion coefficient of O_2 (1.9×10^{-5} cm^2·s^{-1}), and v is the kinetic viscosity of the electrolyte (0.01 cm^2·s^{-1}) .

The hydrogen peroxide yield (H_2O_2-%), and n were evaluated by the rotating ring disk electrode (RRDE) measurements. The potential of the platinum ring electrode was kept at 1.2 V (vs. RHE) and the hydrogen peroxide yield and n were calculated by the following equation:

$$n=\frac{4\times I_{Disk}}{I_{Disk}+I_{Ring}/\mathrm{N}} \quad (3)$$

$$(HO_2^-)\%=\frac{200\times I_{Ring}}{I_{Ring}+I_{Disk}\times\mathrm{N}} \quad (4)$$

where I_{Disk} and I_{Ring} are the measured disk and ring current. N is the ring current collection efficiency (N=0.37).

Zinc-Air Battery Measurements:

The Zn-air battery (ZAB) was assembled by using the zinc foil, catalyst-loaded carbon paper, and 6 M KOH with 0.2 M $ZnCl_2$ solution as the anode, cathode, and electrolyte, respectively. The catalyst loading was 0.9 mg cm^{-2} for Fe_3C/Fe-N-C and Pt/C. The performance of the ZAB was measured on a CHI 760E electrochemical

workstation. The galvanostatic discharge stability for the ZABs was carried out at a current density of 10 mA cm^{-2}.

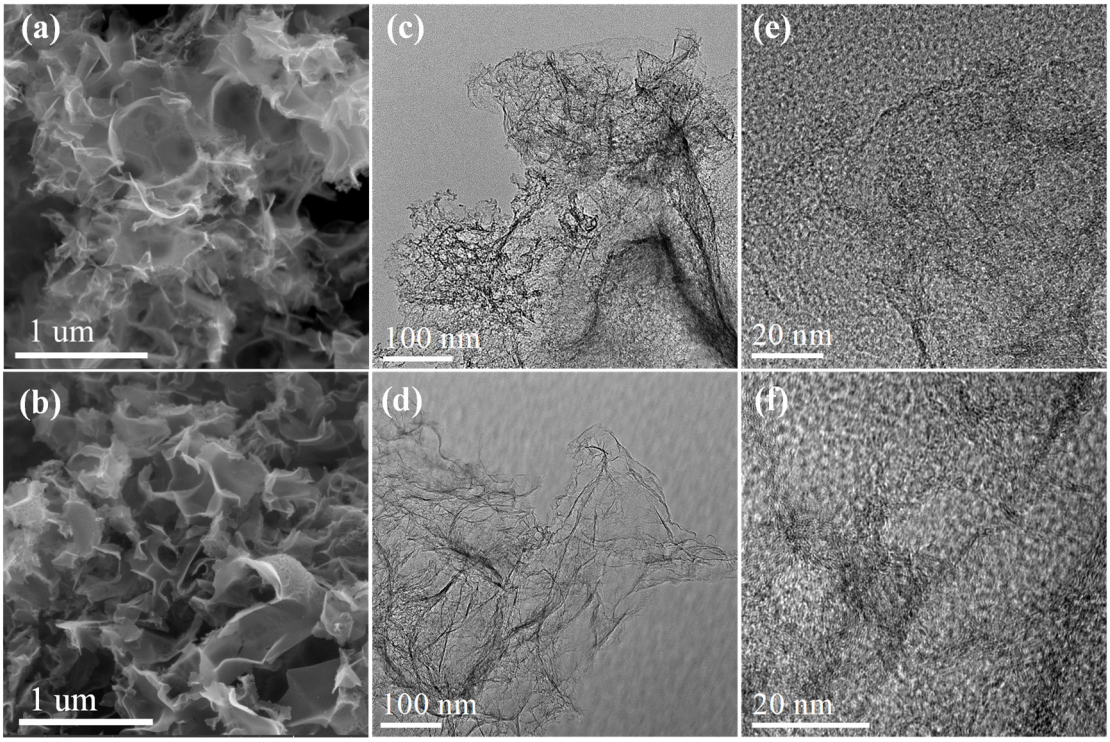

Fig. S1 SEM image of (a) N-C and (b) Fe-N-C, TEM image of (c) N-Cand (d)Fe-N-C, HRTEM image of (e) N-C and (f) Fe-N-C.

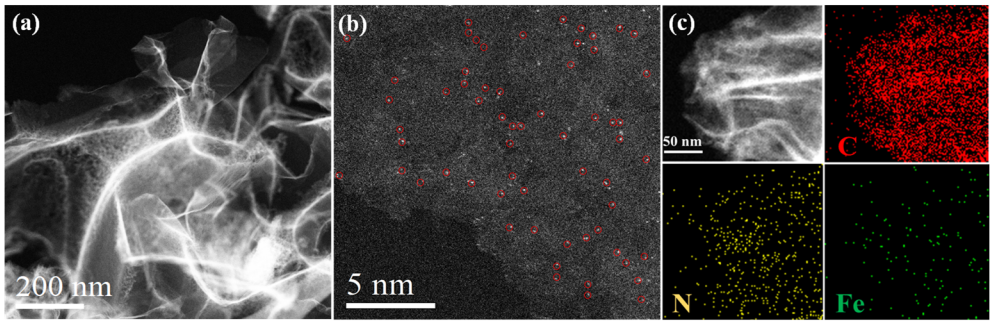

Fig. S2 (a) TEM image of Fe-N-C, (b) high-resolution HAADF-STEM image of Fe-N-C, (c) low-resolution HAADF-STEM image and the corresponding EDS images for C, N, Fe in Fe-N-C.

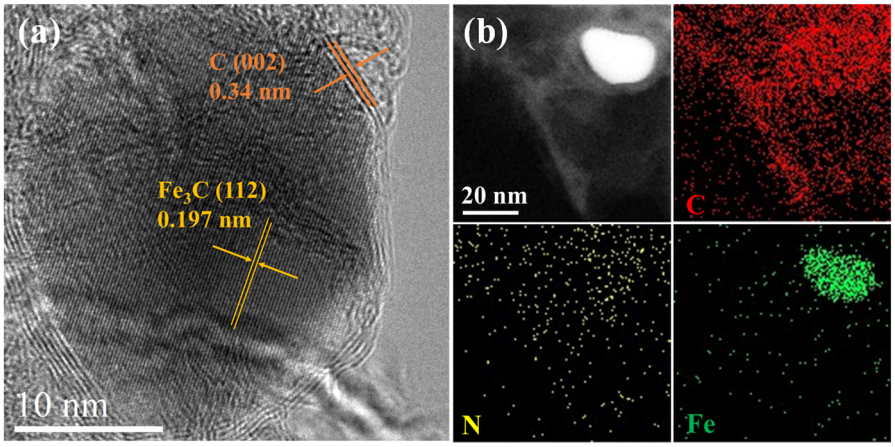

Fig. S3 (a) HAADF-STEM images of Fe_3C/Fe-N-C (isolated Fe sites are highlighted by the red circles), (b) HADDF-STEM image and the element mappings of Fe_3C/Fe-N-C.

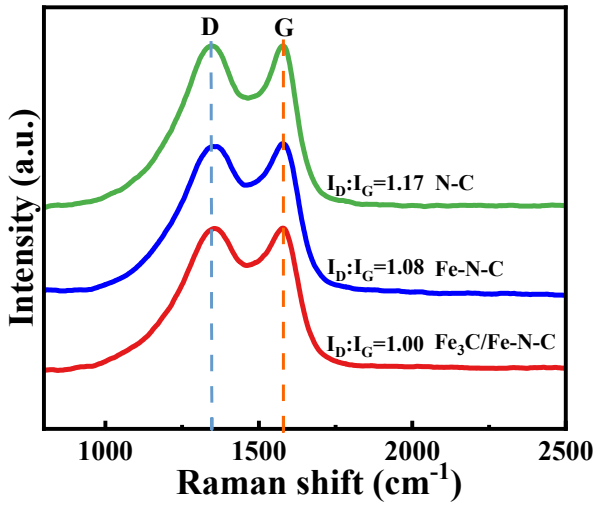

Fig. S4 Raman spectra of N-C, Fe-N-C and Fe_3C/Fe-N-C.

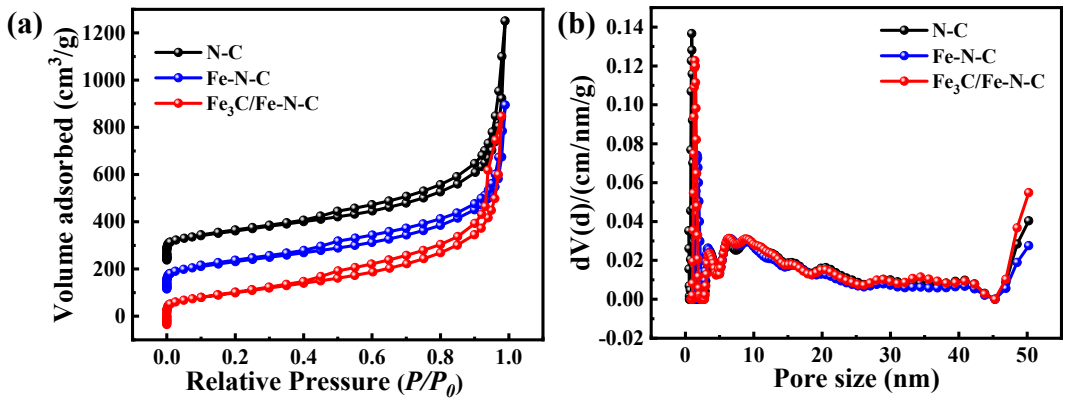

Fig. S5 (a) N_2 adsorption/desorption isotherms of N-C, Fe-N-C and Fe_3C/Fe-N-C, (b) Pore size distribution of N-C, Fe-N-C and Fe_3C/Fe-N-C.

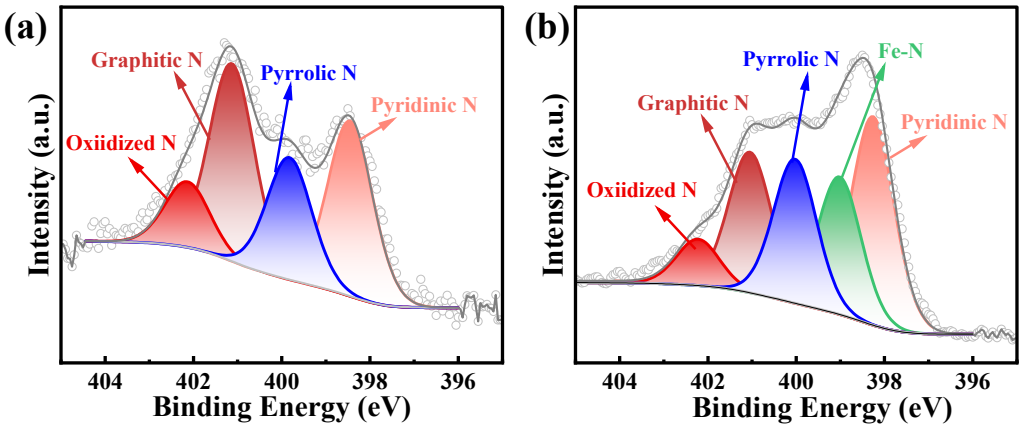

Fig. S6 High-resolution N 1s spectra of (a) N-C and (b) Fe-N-C.

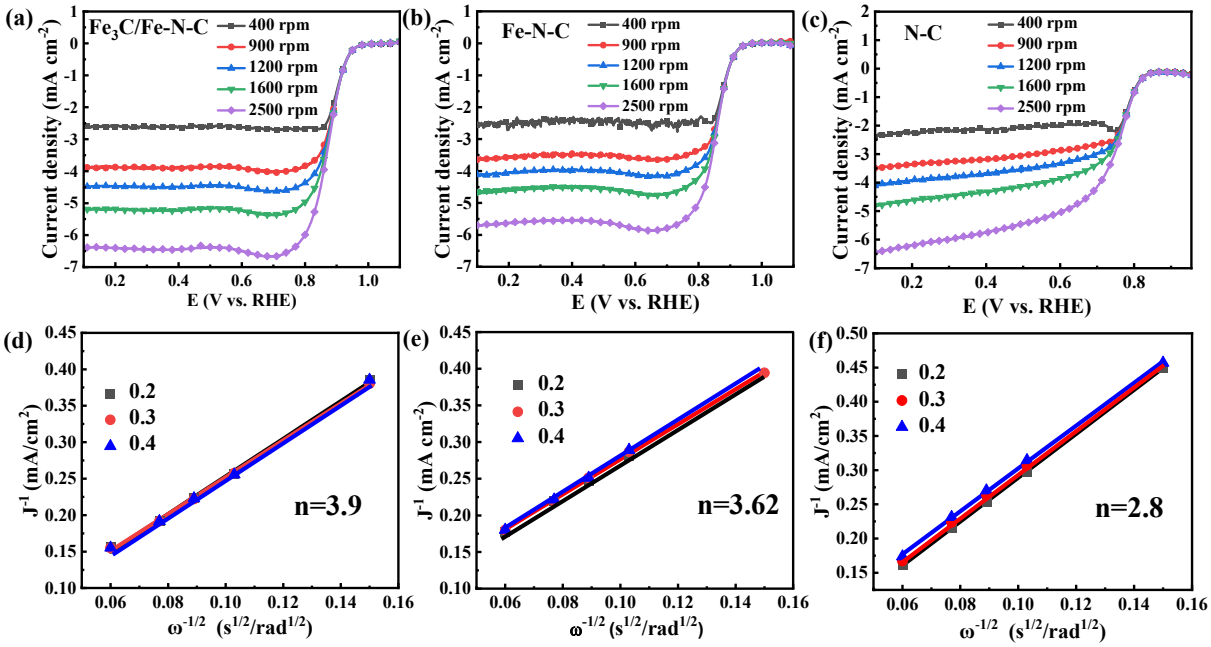

Fig. S7 LSV curves of (a) Fe_3C/Fe-N-C, (b) Fe-N-C and (c) N-C at different rotating rates. (d-f) the corresponding K-L plots.

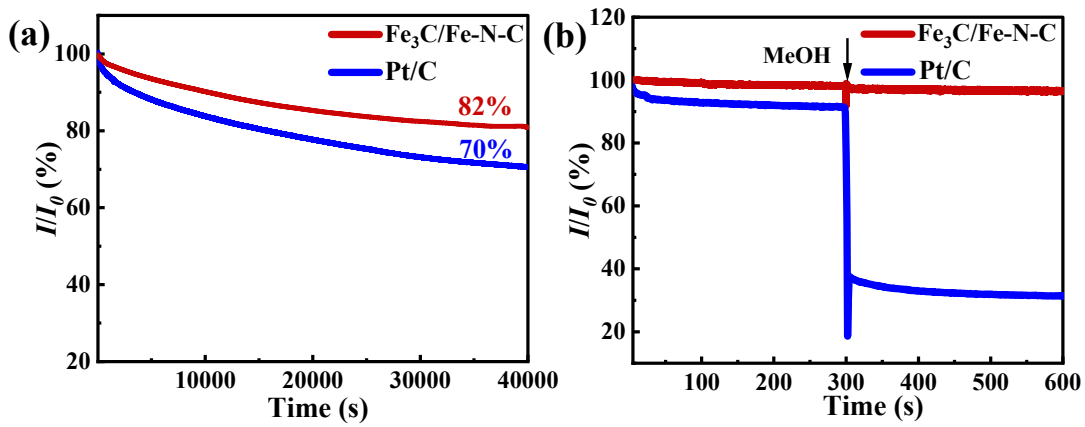

Fig. S8 (a) Stability and (b) methanol tolerance tests for Fe_3C/Fe-N-C and Pt/C.

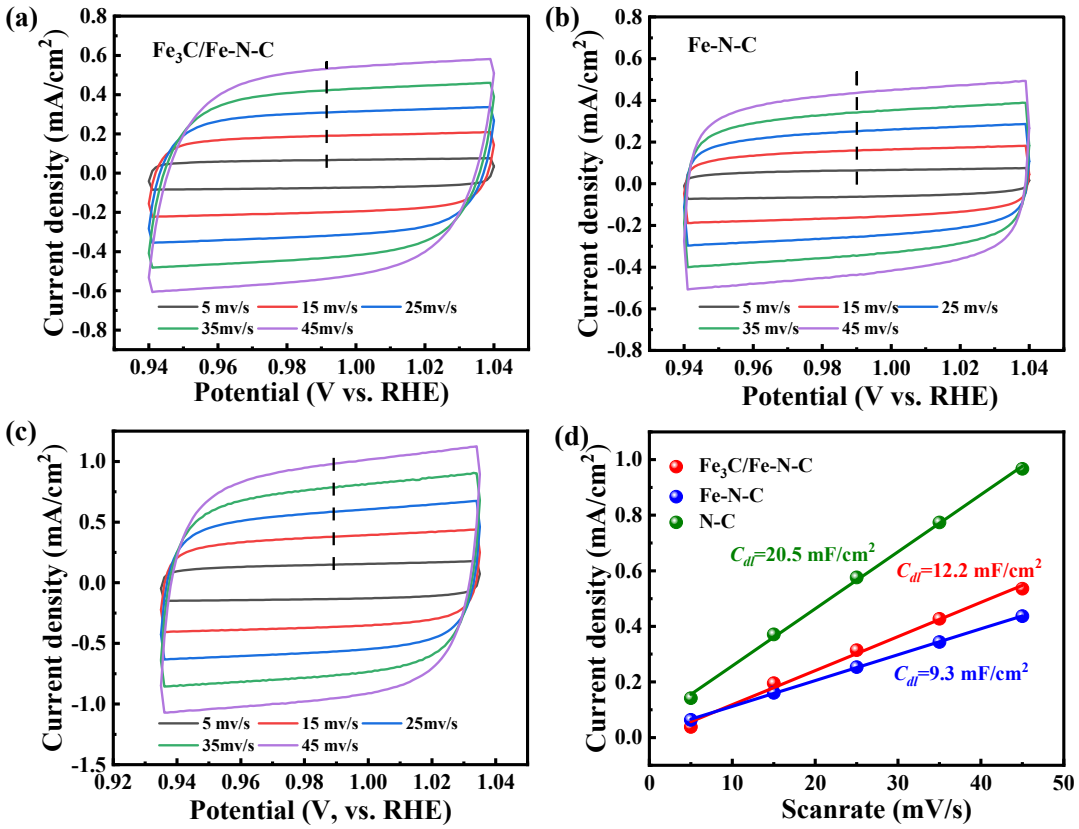

Fig. S9 (a-c) CV curves for various catalysts at 0.94-1.04 V (vs. RHE), (d) Current density as a function of the scan rate for various catalysts.

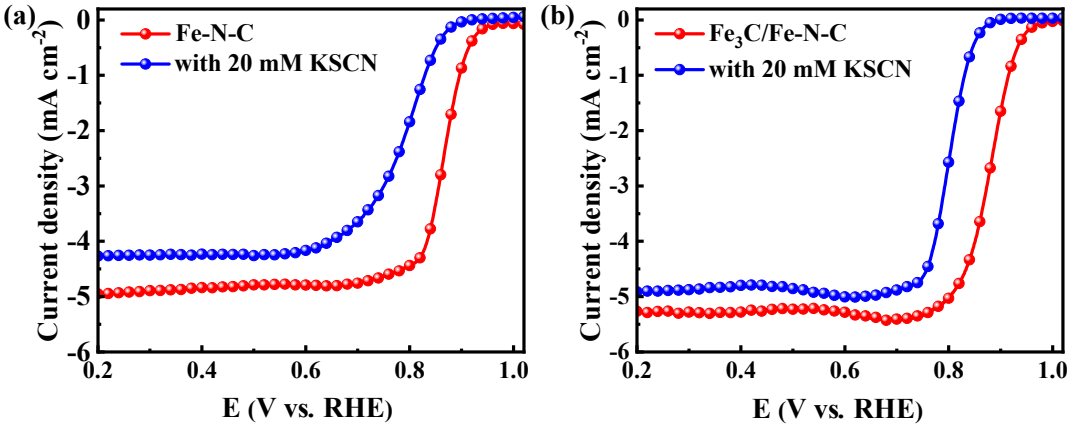

Fig. S10 The LSV curves of (a) Fe-N-C and (b) Fe_3C/Fe-N-C in O_2-saturated 0.1 M KOH electrolyte with and without 20 mM SCN^-.

Table S1. Summary of the Brunauer–Emmett-Teller (BET) surface areas and pore size distributions.

Sample	BET surface area ($m^2 g^{-1}$)	Pore Volume ($cm^3 g^{-1}$)	Pore Diameter (nm)
Fe_3C/Fe-N-C	480.05	1.27	3.83
Fe-N-C	427.19	1.13	3.82
N-C	444.15	1.51	3.81

Table S2. The element atomic contents of C, N and Fe in various catalysts detected by XPS measurement.

Sample	Atomic %		
	C	N	Fe
Fe_3C/Fe-N-C	94.35	5.18	0.47
Fe-N-C	90.41	8.98	0.62
N-C	94.71	5.29	/

Table S3 Comparison of ORR performance and corresponding ZABs power density of recently reported carbon-based catalysts.

Sample	E_{onset} (V vs. RHE)	$E_{1/2}$ (V vs. RHE)	Maximum Power density ($mW \cdot cm^{-2}$)	Reference
Fe_3C/Fe-N-C	0.99	0.89	211	This work
FeNPs/FeSAs-NC	1.03	0.87	/	Appl. Mater. Interfaces 2022, 14, 29986−29992
Fe/Fe_3C@NC-6	0.97	0.86	/	J. Colloid. Interface. Sci. 2023, 949, 169863
Fe_3C@FeSA-NC	/	0.88	164.5	Nano Res. 2023, 16(7): 9371–9378
Fe-NHMCTs	0.99	0.872	/	Adv. Funct. Mater. 2021, 31, 2009197
Fe_3C/N, S-CNS	0.98	0.86	163	Small 2023, 19, 2300136
FeN/C_{60}O-900	0.98	0.85	/	J. Mater. Chem. A 2023, 11, 25534–25544
Fe/Meso-NC-1000	0.97	0.885	109.6	Adv. Mater. 2022, 34, 2107291
Fe SA-NSC-900	0.94	0.86	/	ACS Energy Lett. 2021, 6, 379-386
Fe_3C@MET-M	/	0.84	212	Energy Storage Mater. 56 (2023) 394–402
FeN_3OS	1.01	0.874	/	Angew. Chem. Int. Ed. 2021, 133, 25500-25505
Fe_1-$NS_{1.3}C$	0.97	0.86	/	Angew. Chem. Int. Ed. 2021, 60, 25404-25410
FeNC-SN-2	/	0.89	260	Adv. Funct. Mater. 2021, 31, 2100833
Fe_1-HNC-500-850	/	0.842	/	Adv. Mater. 2020, 32, 1906905
Fe_3C@NCNTs	/	0.84	194	Energy Storage Mater. 2022, 51, 149-158
FeN_4-FeNCP@MCF	/	0.894	208.1	Adv. Funct. Mater. 2024, 2315150
Fe@NCNT-rGO	0.896	0.75	/	Materials 2020, 13, 4144
Fe-N-CNT	0.943	0.811	/	ChemSusChem 2020, 13, 938–944
FeNi-OCNT12	1.01	0.87	/	Waste Manage. 2020, 109, 119–126
FeMn−N−C	1.05	0.92	151	Adv. Mater.

				2024, 36, 2405763
Fe_1/SMC-60	1.05	0.9	223	Green Carbon 2024, 2 ,221–230
Fe-ACSA@NC	1.03	0.9	140	Angew. Chem. Int. Ed. 2022, 61, e202116068
Fe-ZIF-8(CZ-A)	0.93	0.85	/	Green Carbon 2023, 1, 160–169